Polym. Bull. (2011) 67:77–89
DOI 10.1007/s00289-010-0404-9

ORIGINAL PAPER

Effect of org-titanium phosphonate on the properties of chitosan films

Rui Li · Changhua Liu · Jun Ma · Yajuan Yang · Haixia Wu

Received: 11 June 2010 / Revised: 1 November 2010 / Accepted: 6 November 2010 /
Published online: 17 November 2010

Abstract A new type of titanium glycine-*N*,*N*-dimethylphosphonate Ti[$(O_3PCH_2)_2$ NCH_2COOH] (TGDMP), with the functional groups –COOH, has been prepared first and then characterized by Fourier transform infrared spectroscopy (FTIR), X-ray diffraction (XRD), and transmission electron microscopy (TEM). Subsequently, chitosan/titanium glycine-*N*,*N*-dimethylphosphonate (CS/TGDMP-*n*) nanocomposite films of various compositions were prepared by solution casting method. The structure, morphology, and properties of nanocomposite films were investigated by FTIR, XRD, scanning electron microscopy (SEM), thermal gravimetric analysis (TGA), and tensile tests. The results showed that the mechanical properties of chitosan films were improved by the incorporation of TGDMP, and the samples kept at moisture environment showed the larger elongation and lower tensile strength than the dried counterparts. In addition, the CS/TGDMP-*n* films exhibited higher thermal stability and better moisture barrier property than neat CS films.

Keywords Chitosan · Titanium glycine-*N*,*N*-dimethylphosphonate · Nanocomposite films · Properties

Introduction

Chitosan (CS) is the *N*-deacetylated polysaccharide from chitin, and it is also a cationic polymer. Due to its low price, good biocompatibility, biodegradability, non-antigenicity, and multiple functional groups [1–4], CS has been widely used in various fields, such as wastewater treatment [5], separation membrane [6], wound dressing [7], food packaging [8], and so on. However, the poor mechanical

R. Li · C. Liu (✉) · J. Ma · Y. Yang · H. Wu
College of Chemistry and Chemical Engineering, Southwest University,
Chongqing 400715, People's Republic of China
e-mail: chliu@swu.edu.cn

properties, thermal stability, and hydrophilic property restrict its wide-range application.

At present, one way to improve the properties of polymer is blending the nanofillers with matrix, because these composites exhibit greatly improved mechanical properties, enhanced gas barrier properties, fire retardancy, and so on [9–11]. The most common nanofillers are carbon nanotubes, montmorillonites, layered double hydroxides, and phosphates. Although the addition of these nanofillers provides many advantages, they can lead to a loss in same properties of the polymer due to incompatibility between the nanofillers and polymer. For this reason, a number of researchers have focused on using surface modifiers (alkylamines, surfactants, silane coupling agents, etc.) [12–14] or grafting functional groups on nanofillers to enhance the interfacial interaction with polymer matrix [15]. Obviously, these methods are not the simplest to improve the compatibility between the nanofillers and polymer. Furthermore, some researchers reported that the P–OH groups anchored to the layer surface of zirconium phosphate (ZrP) can be replaced with P–OR or P–R groups (R is an organic group) without altering the inorganic texture of the layers [16], which provided a new method for modifying polymers. Therefore, some organic/inorganic hybrid nanomaterials have been applied to modify polymers, such as the preparation of starch/zirconium phosphonate nanocomposite films [17], polyvinylidene fluoride/ZrSPP nanocomposite membranes [18], chitosan/ZrSP composites [19] and epoxy/layered zirconium phosphonate (Zr-P) nanocomposites [20].

On the basis of above described facts, we designed a new material—org-titanium phosphonate, titanium glycine-*N*,*N*-dimethylphosphonate $Ti[(O_3PCH_2)_2NCH_2$-$COOH]$ (TGDMP), as nanofiller. Firstly, titanium phosphate (TiP) has isomorphous structure with zirconium phosphate (ZrP) [21], so P–OH groups of TiP can be replaced with P–OR or P–R groups (R is an organic group). Secondly, the raw materials for titanium phosphonate are low-cost compared with zirconium phosphonate, which will facilitate the practicability of polymer products. Thirdly, TGDMP is the electronegative nanofiller because of the high content of –COOH groups. The electrostatic interactions between nanofillers and chitosan can strengthen interfacial adhesion, which is beneficial to improve the mechanical properties, thermal stability, and moisture barrier property of chitosan.

In this work, we firstly synthesized TGDMP nanofiller by direct precipitation, and then determined the effect of TGDMP fillers on the mechanical properties, thermal stability, and moisture barrier property of chitosan films. Additionally, we investigated the influence of moisture on the mechanical properties.

Experimental

Materials

All the chemicals and reagents used were of analytical grade. Chitosan (CS) was purchased from Nantong Xincheng Biological Industrial Limited Company (Nantong, China) ($M_w = 300{,}000 \pm 50$) and more than 90% degree of deacetylation.

Titanium(IV) chloride ($TiCl_4$) was provided by Tianjin Kermel Chemical Reagent Development Center (Tianjin, China). *N,N*-Bis(phosphonomethyl)-glycin ($(H_3O_3PCH_2)_2NCH_2COOH$, DMPG) was synthesized according to literature [22]. The molecular structure is showed in Fig. 1. Phosphorus(V) oxide was supplied by Chengdu Kelong Chemical Reagent Company (Chengdu, China). Hydrochloric acid and other reagents were purchased from Chongqing Chuandong Chemical Reagent Factory (Chongqing, China). The water used was distilled and deionized.

Preparation of amorphous TGDMP

TGDMP was synthesized according to the previous study [23]. 430 mL of 2 M HCl containing 0.3 M $TiCl_4$ was slowly added to 400 mL of 0.63 M *N,N*-bis(phosphonomethyl)-glycin. After 24 h, the precipitate was filtered, washed with distilled water to pH = 3–3.5, and dried over P_2O_5.

Preparation of CS/TGDMP-*n* nanocomposite films

The chitosan solution was prepared by dissolving 2 g of CS in a 100 mL of aqueous acetic acid solution (2% v/v) with stirring. Then the dispersed TGDMP suspension (0.5 wt%) was added dropwise to this solution with the loading of nanofillers from 0.2 to 1.0 wt% (based on the chitosan weight). The mixture was stirred at 60 °C for 3 h. After degassing under vacuum, the CS/TGDMP solution was poured into a glass plate and heated at 50 °C to obtain dry films. A series of nanocomposite films were prepared and coded as CS/TGDMP-*n* (where *n* represents the different TGDMP loadings). In order to compare with the CS/TGDMP-*n* films, neat CS film was obtained through the same experiment process, which was coded as CS. The samples were conditioned in a desiccator at 43% RH (relative humidity) before conducting FTIR, XRD, SEM. The codes of samples were listed in Table 1.

Characterization

Fourier transform infrared (FTIR) spectra of TGDMP and the blend films were recorded on a Nicolet (Madison, WI, USA) 170SX Fourier transform infrared

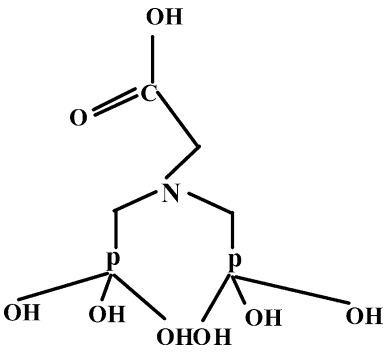

Fig. 1 The molecular structure of DMPG

Table 1 Codes of the samples

Samples	CS	CS/TGDMP-1	CS/TGDMP-2	CS/TGDMP-3	CS/TGDMP-4	CS/TGDMP-5
TGDMP content (wt%)	0	0.2	0.4	0.6	0.8	1.0

spectrometer in the wavelength range of 4000–500 cm^{-1} in the attenuated total reflection mode.

X-ray diffraction (XRD) patterns of the samples were recorded on an X-ray diffractometer (XRD-3D, PuXi, BeiJing, China) at a voltage of 36 kV and a current of 20 mA using Cu Kα radiation ($\lambda = 0.15406$ nm). The scanning rate was 4°/min and the scanning scope of 2θ was 3°–50° at room temperature.

Transmission electron microscopy (TEM) image of TGDMP powder was obtained on a JEM-100CXII instrument (Japan) with an accelerating voltage of 80 kV.

The morphologies of cross-sections of the films were observed on a scanning electron microscope (S-4800, HITACHI, Japan). Before testing, the samples were fractured with liquid nitrogen and coated with gold in a 13.3 Pa vacuum degree.

Thermogravimetric analysis (TGA) of the CS/TGDMP-*n* nanocomposite films was performed using a TA-STDQ600 (TA Instruments Inc, New Castle, USA). The thermograms were acquired between 25 and 500 °C at a heating rate of 10 °C/min. The experiment was carried out in nitrogen environment using a flow rate 20 mL/min in order to avoid thermoxidative degradation. An empty pan was used as a reference.

The tensile strength (σ_b) and elongation at break (ε_b) of the blend films were tested using a Micro-electronics Universal Testing Instrument Model Sans 6500 (Shenzhen Sans Testing Machine Co. Ltd, Shenzhen, China) with the cross-head speed was 10 mm/min. According to the Chinese standard method (GB 13022-91), all the films were cut into 10 × 100 mm (width × length) strips and mounted between cardboard grips (150 × 300 mm) using adhesive so that the final area exposed was 10 × 50 mm. Before testing, the samples were equilibrated at 0, 43, and 98% RH for more than 1 week at room temperature, respectively. The average value of σ_b and ε_b was set as the representative value.

The moisture uptake of CS/TGDMP-*n* nanocomposite films was determined. The samples used were thin rectangular strips with dimensions of 50 × 10 × 0.1 mm. The initial dry nanocomposite films were determined by drying to constant weight in an oven at 80 °C. After weighing, they were equilibrated at 43% RH and 98% RH, respectively. The samples were removed at desired intervals and weighed until the equilibrium state was reached. The moisture uptake (Mu) of the samples was calculated as follows:

$$\mathrm{Mu} = (W_1 - W_0) / W_0 \times 100\%$$

where W_0 and W_1 were the weight of samples before and after exposure to 43% RH or 98% RH, respectively. Each moisture uptake experiment was repeated three times, and the average values were reported.

Results and discussion

FTIR analysis

The FTIR spectra of TGDMP powder and CS/TGDMP-*n* nanocomposite films are shown in Fig. 2. In the spectrum of TGDMP (Fig. 2a), the broad band at 3444 cm^{-1} was attributed to adsorbed moisture and hydrogen bonding between the carboxylic acid groups [24]. The sharp peaks at 1735 and 1638 cm^{-1} were assigned to –COOH and $–COO^-$ stretching vibrations [24, 25]. The strong bands in the range 1000–1200 cm^{-1} were characteristic of phosphate groups [26, 27]. And the weak band at 612 cm^{-1} corresponded to the deformation vibration for the Ti–O bond [28]. These obvious characteristic peaks indicated that the TGDMP had been synthesized successfully.

The FTIR spectra of neat CS film and CS/TGDMP-3 nanocomposite films are shown in Fig. 2b. For neat CS, the broad band at 3194 cm^{-1} was the OH stretching, which overlapped the N–H stretching in this region [29]. The peak around 2862 cm^{-1} was typical C–H stretching vibrations [30]. The small peak at 1634 cm^{-1} was assigned to C=O stretching vibrations (amide I) [31], and the band at 1538 cm^{-1} was the N–H bending (amide II). The peak at 1405 cm^{-1} corresponded to stretching of carboxylate anions, which was attributed to CS dissolved in acetic acid solution [32].

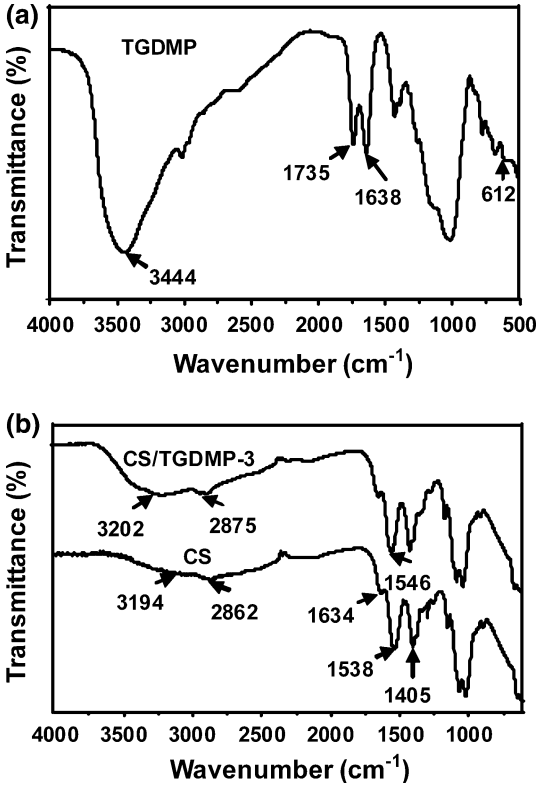

Fig. 2 FTIR spectra of **a** TGDMP powder, **b** CS and CS/TGDMP-3 nanocomposite films

After the formation of CS/TGDMP-3 nanocomposite films, it was found that the characteristic peaks at 3194, 2862, and 1538 cm^{-1} of CS shifted to 3202, 2875, and 1546 cm^{-1}, respectively. These changes could be attributed to hydrogen bonding and electrostatic interactions between TGDMP and CS.

X-ray diffraction analysis

XRD patterns of pristine TGDMP and films are shown in Fig. 3. As seen from the X-ray diffractograms, the broad peak indicated TGDMP nanofillers were amorphous. The X-ray pattern of neat CS film showed three characteristic peaks located at 2θ about 11.64°, 18.32°, and 23.46°, which was in agreement with the previous report [33]. The crystalline peaks at 11.64°, 18.32° (2θ) were ascribed to the hydrated and anhydrous crystalline structure, while the broad peak around 23.46° (2θ) indicated the existence of an amorphous structure [34]. Compared with neat CS, the CS/TGDMP-*n* nanocomposite films almost showed the similar XRD patterns except the intensity of the diffraction peaks at 11.64° and 18.32° became a little bit weaker and wider, especially for the CS/TGDMP-2 film. This result indicated that the crystallization of CS was inhibited by the loading of TGDMP, and the best compatibility existed in the nanocomposite films with 0.4 wt% TGDMP. At the same time, no characteristic diffraction peak for TGDMP was found in the nanocomposite films, probably due to the low loading amorphous TGDMP.

Morphological image analysis

The morphologies of as-synthesized materials are studied by TEM and SEM. TEM image in Fig. 4 showed that the size of TGDMP particles was nano-scale and no layered

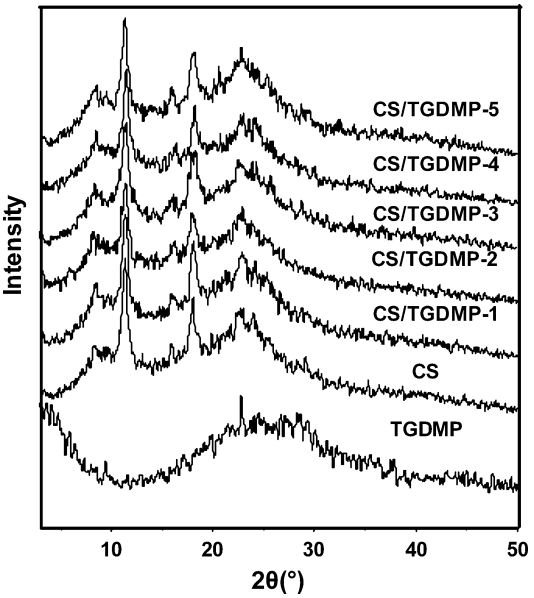

Fig. 3 XRD patterns of the TGDMP, CS and CS/TGDMP-*n* nanocomposite films

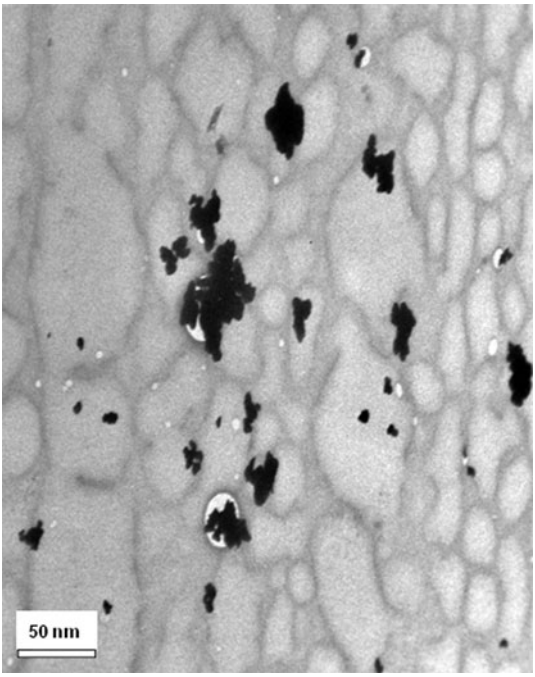

Fig. 4 TEM image of TGDMP powder

structure was found, indicating their features were amorphous not crystalline, which was also proved by XRD (Fig. 3). One could also see some particles were aggregated in clusters, but the size was still less than 100 nm, which testified that the CS/TGDMP-*n* films were true nanocomposites. Furthermore, to observe the cross-sections of CS and blend films, the SEM micrographs were displayed. As shown in Fig. 5, neat CS film exhibited a smooth and compact surface, and the nanofillers were dispersed uniformly in the CS/TGDMP-1 and CS/TGDMP-2 films, which suggested a good compatibility between TGDMP and chitosan. This could be attributed to plenty of carboxylic acid groups on the surface of TGDMP, which were easy to form strong electrostatic interactions and hydrogen bonding with chitosan molecules. Additionally, several holes occurred on the fracture surface of the CS/TGDMP-1 film, which might come from residual bubbles in the chitosan solution before casting. However, the rougher fracture surface could be seen in the CS/TGDMP-4 film, which was presumably due to the poor dispersion and aggregations of TGDMP at high loading. This could account for why the mechanical properties became worse at high TGDMP loading.

Thermogravimetric analysis

In order to determine the thermal stability of neat CS and composite films, thermogravimetric analysis was carried out. As can be seen from Fig. 6, the first weight loss between 30 and 165 °C was attributed to the loss of absorbed water. The second stage of the weight loss in the temperature range of 200–360 °C corresponded

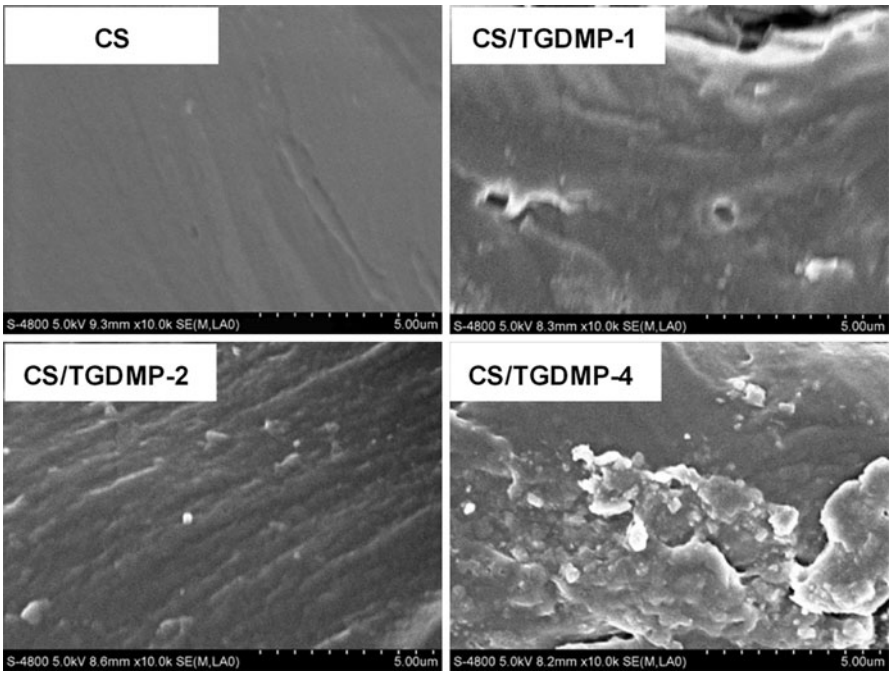

Fig. 5 SEM micrographs CS and CS/TGDMP-*n* nanocomposite films

to the degradation and deacetylation of chitosan. These results agreed with the former literature [35, 36]. An improvement in the thermal stability of the nanocomposite films could be seen with an increase of nanofillers loading. For example, the decomposed residual weight of CS/TGDMP-*n* films increased in comparison with neat CS. Meanwhile, it is generally accepted that reliable degradation temperature, such as the initial decomposed temperature (IDT) [37], the temperature at 50% weight loss ($T_{-50\%}$), the integral procedural decomposition temperature (IPDT) [38], and the final decomposed temperature (FDT) [37], can be used to assess a material's lifetime. All experimental results of TGA were listed in Table 2. These results indicated that the degradation temperatures of the CS/TGDMP-*n*, including IDT, $T_{-50\%}$, IPDT, and FDT, increased by adding TGDMP in the chitosan matrix. The fact may be explained as follows: Firstly, due to the strong electrostatic and hydrogen bonding interactions with the chitosan, TGDMP nanofillers acted as barriers that restrained the mobility of CS chains. Secondly, TGDMP nanofillers acted as an insulator which hindered heat-transfer between the CS molecular chains.

Mechanical properties analysis

The effect of TGDMP loading on the mechanical properties of chitosan films, at different RH, is shown in Fig. 7. It was found that, with increasing RH, all the films showed larger elongation at break (ε_b) and lower tensile strength (σ_b). For example, when RH changed from 0 to 98%, the σ_b and ε_b of CS/TGDMP-2 film changed from

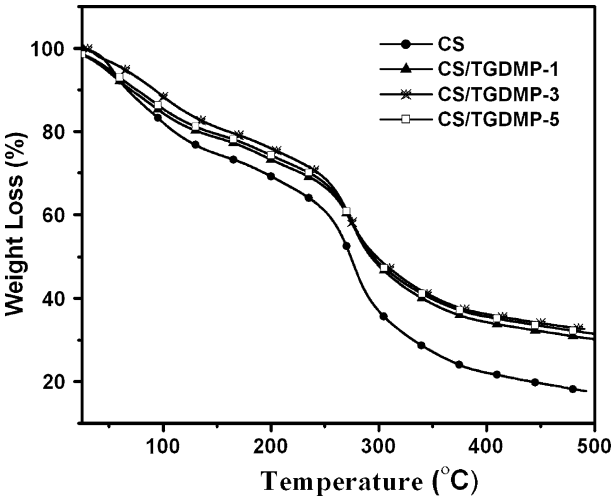

Fig. 6 TGA curves of CS and CS/TGDMP-*n* nanocomposite films

Table 2 Thermal analysis of neat CS and CS/TGDMP-*n* nanocomposite films measured by TGA

Sample	IDT (°C)	FDT (°C)	IPDT (°C)	$T_{-50\%}$ (°C)
CS	250.41	313.75	224.69	273.8
CS/TGDMP-1	254.73	319.34	387.03	298.0
CS/TGDMP-3	257.05	328.52	411.75	298.0
CS/TGDMP-5	257.47	333.04	408.61	294.6

87.9 MPa, 21.8% to 17.7 MPa, 85.8%, respectively. This result may be due to the moisture up-take. Since water molecules served as plasticizer, they could weak the intermolecular forces between CS chains and the bonding strength between nanofillers and matrix [39].

In the case of the tensile strength, it was found that, at the same RH, the σ_b of composite films showed a higher value than that of neat CS film. For instance, at 43% RH, the σ_b of chitosan was increased from 37.26 to 45.06 MPa by the addition of TGDMP. These results suggested that TGDMP as nanofillers could improve the strength of chitosan, which was similar to previous reports about polymer/nanofiller [40–42]. The improvement in the tensile strength was due to (i) nanofillers were dispersed well within the polymer matrix; (ii) since TGDMP nanofillers had strong hydrogen bonding and electrostatic interactions with chitosan, they were difficult to disconnect from the matrix when the composites were under tensile stress, and could resist and transfer the imposed force, leading to the dispersion of the tensile energy into surrounding matrix. However, when adding higher amount of TGDMP, the dispersion of TGDMP was poor and the aggregations formed in the nanocomposite films, which was supported by the SEM micrographs discussed above. Therefore, the tensile strength decreased. In addition, it was observed that the

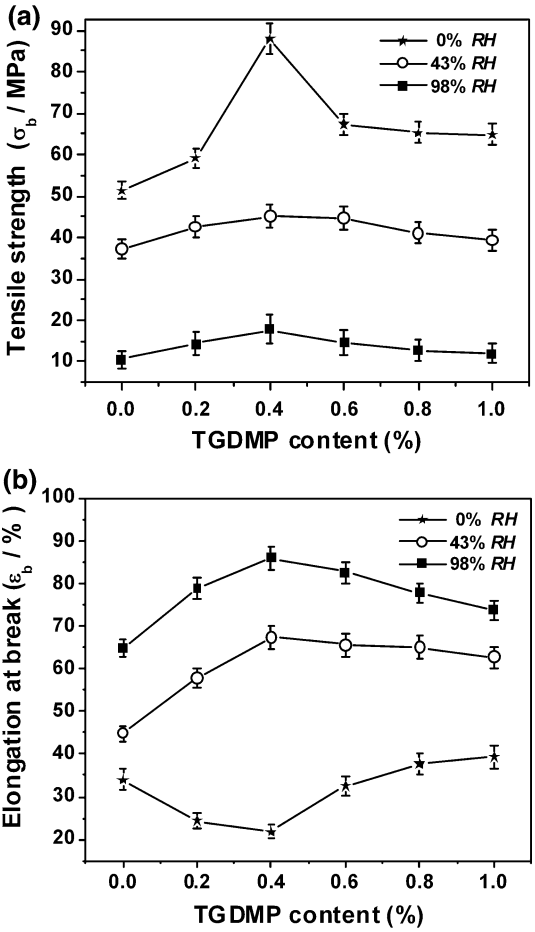

Fig. 7 The mechanical properties of CS and CS/TGDMP-*n* nanocomposite films under different relative humidity **a** the tensile strength, **b** the elongation at break

CS/TGDMP-*n* films exposed to moisture performed better in elongation at break than neat CS, which was attributed to the synergistic effect of nanofillers and water molecules. But the behavior of dry samples was different, they were easier to fracture, similar result has been reported [43].

From the above results, it appeared that an optimal amount of TGDMP (0.4 wt%) was necessary to achieve the greatest improvement of mechanical properties, and the influence of moisture on the mechanical properties of chitosan films could not be neglected.

Moisture uptake of the films analysis

Water sensitivity is another important property for practical applications of chitosan films. In order to analyze the moisture barrier property, the moisture uptake (Mu) for

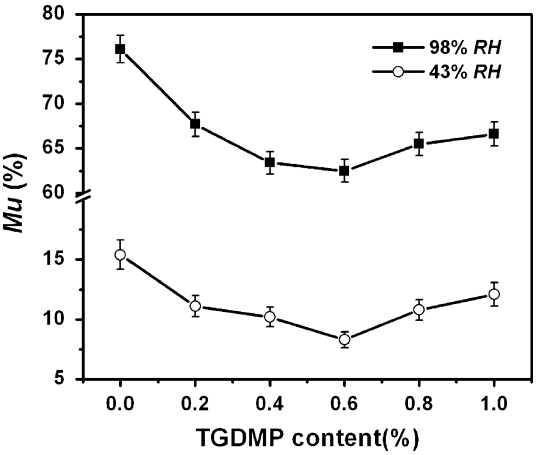

Fig. 8 Moisture uptake (Mu) of CS and CS/TGDMP-*n* nanocomposite films at different relative humidity

nanocomposite films at 43% RH and 98% RH was tested, respectively. As seen from Fig. 8, the Mu for all samples increased when RH changed from 43 to 98%. But, at the same RH, the Mu for composite films decreased compared to neat chitosan. When the loading of TGDMP was 0.6 wt%, the Mu for composite films reached minimum value. The improvement of moisture barrier property might be caused by the strong electrostatic and hydrogen bonding interactions between CS and TGDMP, decreasing the number of –OH or $–NH_2$ groups of CS available for interaction with migrating water molecules. In other words, it could reduce the adsorption of water molecules on the surface of CS films. However, the Mu increased when TGDMP loading was more than 0.6 wt%. This could be attributed to aggregations of nanofillers, which weakened the interactions between CS and TGDMP, increasing number of available –OH or $–NH_2$ groups. On the whole, the Mu values for nanocomposite films were lower than that for neat CS. These results indicated that the presence of TGDMP improved the moisture resistance of chitosan.

Conclusions

In this paper, the high-performance CS/TGDMP-*n* nanocomposite films have been successfully prepared by solution casting method. Results from FTIR indicated that TGDMP had formed strong electrostatic and hydrogen bonding interactions with CS, which resulted in better compatibility between them. Tensile testing showed that the CS/TGDMP-*n* films had higher tensile strength and larger elongation at break than neat chitosan at 43% RH and 98% RH, and the influence of moisture on the mechanical properties of chitosan films could not be neglected. In addition, TGA and Mu studies showed the composite films exhibited superior to neat chitosan in the thermal stability and resistance to moisture absorption.

References

1. Lee EJ, Shin DS, Kim HE, Kim HW, Koh YH, Jang JH (2009) Membrane of hybrid chitosan–silica xerogel for guided bone regeneration. Biomaterials 30:743–750
2. Zhang XD, Yang DZ, Nie J (2008) Chitosan/polyethylene glycol diacrylate films as potential wound dressing material. Int J Biol Macromol 43:456–462
3. Jiang LY, Li YB, Wang XJ, Zhang L, Wen JQ, Gong M (2008) Preparation and properties of nano-hydroxyapatite/chitosan/carboxymethyl cellulose composite scaffold. Carbohydr Polym 74:680–684
4. Wan Y, Wu H, Cao XY, Dalai SQ (2008) Compressive mechanical properties and biodegradability of porous poly(caprolactone)/chitosan scaffolds. Polym Degrad Stab 93:1736–1741
5. Kang DW, Choi HR, Keon DK (1999) Stability constants of amidoximated chitosan-g-poly(acrylonitrile) copolymer for heavy metal ions. J Appl Polym Sci 73:469–476
6. Won W, Feng X, Lawless D (2002) Pervaporation with chitosan membranes: separation of dimethyl carbonate/methanol/water mixtures. J Memb Sci 209:493–508
7. Mi FL, Shyu SS, Wu YB, Lee ST, Shyong JY, Huang RN (2001) Fabrication and characterization of a sponge-like asymmetric chitosan membrane as a wound dressing. Biomaterials 22:165–173
8. Dutta PK, Tripathi S, Mehrotra GK, Dutta J (2009) Perspectives for chitosan based antimicrobial films in food applications. Food Chem 114:1173–1182
9. Jo BW, Park SK, Kim DK (2008) Mechanical properties of nano-MMT reinforced polymer composite and polymer concrete. Constr Build Mater 22:14–20
10. Kong Y, Du HW, Yang JR, Shi DQ, Wang YF, Zhang YY, Xin W (2002) Study on polyimide/TiO_2 nanocomposite membranes for gas separation. Desalination 146:49–55
11. Wang DY, Liu XQ, Wang JS, Wang YZ, Stec AA, Hull TR (2009) Preparation and characterisation of a novel fire retardant PET/α-zirconium phosphate nanocomposite. Polym Degrad Stab 94:544–549
12. Liu CH, Yang YJ (2009) Effects of α-zirconium phosphate aspect ratio on the properties of polyvinyl alcohol nanocomposites. Polym Test 28:801–807
13. Suguna Lakshmi M, Narmadha B, Reddy BSR (2008) Enhanced thermal stability and structural characteristics of different MMT-clay/epoxy-nanocomposite materials. Polym Degrad Stab 93:201–213
14. Wang LH, Sheng J (2005) Preparation and properties of polypropylene/org-attapulgite nanocomposites. Polymer 46:6243–6249
15. Chakoli AN, Wan J, Feng JT, Amirian M, Sui JH, Cai W (2009) Functionalization of multiwalled carbon nanotubes for reinforcing of poly(L-lactide-co-e-caprolactone) biodegradable copolymers. Appl Surf Sci 256:170–177
16. Bellezza F, Cipiciani A, Costantino U, Negozio ME (2002) Zirconium phosphate and modified zirconium phosphates as supports of lipase. Preparation of the composites and activity of the supported enzyme. Langmuir 18:8737–8742
17. Wu HX, Liu CH, Yang YJ, Chen JG, Chang PR, Chen Y (2010) Starch-based nanocomposites reinforced with layered zirconium phosphonate. Polym Compos. doi:10.1002/pc
18. Casciola M, Alberti G, Ciarletta A, Cruccolini A, Piaggio P, Pica M (2005) Nanocomposite membranes made of zirconium phosphate sulfophenylenphosphonate dispersed in polyvinylidene fluoride: preparation and proton conductivity. Solid State Ionics 176:2985–2989
19. Yang YJ, Liu CH, Wu HX, Li R (2010) Preparation and characterization of films based on zirconium sulfophenyl phosphonate and chitosan. Carbohydr Res 345:148–153
20. Tsai TY, Wu YJ, Hsu FJ (2008) Synthesis and properties of epoxy/layered zirconium phosphonate (Zr-P) nanocomposites. J Phys Chem Solids 69:1379–1382
21. Robert CT, Slade JA, Knowles DJ, Jones JR (1997) The isomorphous acid salts α-$Zr(HPO_4)_2{\cdot}H_2O$, α-$Ti(HPO_4)_2{\cdot}H_2O$ and α-$Zr(HAsO_4)_2{\cdot}H_2O$. Solid State Ionics 96:9–19
22. Moedritzer K, Riyad R (1996) The direct synthesis of α-aminomethylphosphonic acids. J Org Chem 31:1603–1607
23. Alberti G, Cardini-galli P, Costantino U, Torracca E (1967) Crystalline insoluble salts of polybasic metals—ion-exchange properties of crystalline titanium phosphate. J Inorg Nucl Chem 29:571–578
24. Jaimez E, Hix GB, Slade RCT (1997) A phosphate-phosphonate of titanium(IV) prepared from phosphonomethyliminodiacetic acid: characterisation, n-alkylamine intercalation and proton conductivity. Solid State Ionics 97:195–201

25. Warren HJ, Hogarth SS, Muir AK, Whittaker JC, Costa DD, Drennan J, (Max) Lu GQ (2007) Proton conduction mechanism and the stability of sol–gel titanium phosphates. Solid State Ionics 177:3389–3394
26. Misaelides P, Sarri S, Zamboulis D, Gallios G, Zhuravlev I, Strelko VV (2006) Separation of europium from aqueous solutions using Al^{3+}- and Fe^{3+}-doped zirconium and titanium phosphates. J Radioanal Nucl Chem 268:53–58
27. Thakkar R, Chudasama U (2009) Synthesis, characterization and proton transport properties of a mixed material—zirconium titanium phosphate, a tetravalent bimetallic acid salt. Electrochim Acta 54:2720–2726
28. Jia K, Pan BC, Zhang QR, Zhang WM, Jiang PJ, Hong CH, Pan BJ, Zhang QX (2008) Adsorption of Pb^{2+}, Zn^{2+}, and Cd^{2+} from waters by amorphous titanium phosphate. J Colloid Interface Sci 318:160–166
29. Kim IY, Yoo MK, Kim BC, Kim SK, Lee HC, Cho CS (2006) Preparation of semi-interpenetrating polymer networks composed of chitosan and poloxamer. Int J Biol Macromol 38:51–58
30. Wang T, Turhan M, Gunasekaran S (2004) Selected properties of pH-sensitive, biodegradable chitosan–poly(vinyl alcohol) hydrogel. Polym Int 53:911–918
31. Yeh JT, Chen CL, Huang KS (2007) Synthesis and properties of chitosan/SiO_2 hybrid materials. Mater Lett 61:1292–1295
32. Puttipipatkhachorn S, Nunthanid J, Yamamoto K, Peck GE (2001) Drug physical state and drug–polymer interaction on drug release from chitosan matrix films. J Control Release 75:143–153
33. Jayakumar R, Nagahama H, Furuike T, Tamura H (2008) Synthesis of phosphorylated chitosan by novel method and its characterization. Int J Biol Macromol 42:335–339
34. Wang SF, Shen L, Zhang WD, Tong YJ (2005) Preparation and mechanical properties of chitosan/carbon nanotubes composites. Biomacromolecules 6:3067–3072
35. Chen CH, Wang FY, Mao CF, Liao W, Hsieh CD (2008) Studies of chitosan: II. Preparation and characterization of chitosan/poly(vinyl alcohol)/gelatin ternary blend films. Int J Biol Macromol 43:37–42
36. Yang JM, Su WY, Leu TL, Yang MC (2004) Evaluation of chitosan/PVA blended hydrogel membranes. J Memb Sci 236:39–51
37. Khurana P, Aggarwal S, Narulal AK, Choudhary V (2003) Studies on the curing and thermal behaviour of DGEBA in the presence of bis(4-carboxyphenyl) dimethyl silane. Polym Int 52:908–917
38. Park SJ, Kim HC (2001) Thermal stability and toughening of epoxy resin with polysulfone resin. J Polym Sci Polym Phys 39:121–128
39. Chen HY, Miao MG, Ding X (2009) Influence of moisture absorption on the interfacial strength of bamboo/vinyl ester composites. Compos Part A 40:2013–2019
40. Yang YJ, Liu CH, Wu HX (2009) Preparation and properties of poly(vinyl alcohol)/exfoliated α-zirconium phosphate nanocomposite films. Polym Test 28:371–377
41. Wu HX, Liu CH, Chen JG, Chang PR, Chen Y, Anderson DP (2009) Structure and properties of starch/α-zirconium phosphate nanocomposite films. Carbohydr Polym 77:358–364
42. Shieh YT, Yang YF (2006) Significant improvements in mechanical property and water stability of chitosan by carbon nanotubes. Eur Polym J 42:3162–3170
43. Goodridge RD, Hague RJM, Tuck CJ (2010) Effect of long-term ageing on the tensile properties of a polyamide 12 laser sintering material. Polym Test 29:483–493